Radiation Measurements 119 (2018) 85–92

Contents lists available at ScienceDirect

Radiation Measurements

journal homepage: www.elsevier.com/locate/radmeas

Development of a Si-PM-based GGAG radiation-imaging detector with pulse-shape discrimination capability to separate different types of radiation

Seiichi Yamamoto[a,*], Hideo Nitta[b]

[a] Radiological and Medical Laboratory Sciences, Nagoya University Graduate School of Medicine, Japan
[b] Hitachi Metals, Ltd., Japan

ARTICLE INFO

Keywords:
GGAG
Si-PM array
Spatial resolution
Energy resolution
Scintillation decay curve
Pulse shape discrimination

ABSTRACT

We previously developed a radiation detector using a ceramic scintillator made for X-ray computed tomography (CT), $Gd_3(GaAl)_5O_{12}$:Ce (GGAG), combined with a position-sensitive photomultiplier tube (PSPMT) for the imaging of radiation. However, GGAG's scintillation wavelength is more suitable for silicon-based photodetectors than PSPMT, and so better performance is expected by combining it with a silicon-based photodetector. Therefore, here we combined a GGAG plate with silicon photomultiplier (Si-PM) arrays to develop a radiation-imaging detector. Our proposed Si-PM-based GGAG radiation-imaging detector consists of a 0.5-mm-thick GGAG plate, a light guide, and an 8 x 8 Si-PM array. The spatial resolutions of this imaging detector surpassed 0.31-mm FWHM for 5.5-MeV alpha particles. The spatial resolution of the Sr-Y-90 beta particles (maximum energy: 2.28 MeV) was ~0.8 mm FWHM and 0.6-mm FWHM for Ca-45 (maximum energy: 0.24 MeV). The spatial resolutions for Co-57 (122 keV), Am-241 gamma photons (60 keV), and Cs-137 X-rays (~35 keV) were 0.6-, 0.8-, and 1.0-mm FWHM, respectively. Since GGAG's scintillation decay curves for alpha particles are different from gamma photons or beta particles, we can use pulse-shape discrimination to separate the Am-241 alpha particles from the Cs-137 gamma photons as well as from the Sr-Y-90 beta particles.

1. Introduction

Event-by-event type radiation imaging detectors, such as alpha cameras, require a low-cost, high-light-output, and short-decay-time scintillator. We came to view the ceramic scintillator developed for X-ray computed tomography (CT), $Gd_3(GaAl)_5O_{12}$:Ce (GGAG), as a promising candidate, and thus we developed a radiation detector using a GGAG plate combined with a position-sensitive photomultiplier tube (PSPMT) for the imaging of radiation (Yamamoto and Nitta, 2018). The performance of the PSPMT-based GGAG imaging detector for Am-241 alpha particles (5.5 MeV) with a spatial resolution of ~0.53-mm FWHM (Yamamoto and Nitta, 2018) surpassed that with a single-crystal GAGG imaging detector (Morishita et al., 2014, 2017).

However, GGAG's scintillation wavelength is more suitable for silicon photodetectors than PSPMT (Hitachi-Metal data sheet), and so we expect to improve performance by combining them. Therefore, we combined a GGAG plate with silicon photomultiplier (Si-PM) arrays to develop a new radiation imaging detector. So far, many Si-PM based radiation imaging detectors have been developed for positron emission tomography (PET) systems (Yamamoto et al., 2010, 2013, 2016; Kishimoto et al., 2013; Schaart et al., 2009; Yamaya et al., 2011; Yoon et al., 2012; Kwon et al., 2011), single-photon emission tomography (SPECT) systems (Yamamoto et al., 2011), and alpha particles (Morishita et al., 2014, 2017). In the alpha particle imaging detectors using Si-PM arrays for plutonium (Pu) particle detection (Morishita et al., 2014, 2017), higher spatial resolution is required to distinguish the alpha particles of Pu from those emitted by the environmental radon and its daughters. Furthermore, during detection of Pu alpha particles, environmental beta and gamma photons are also detected, increasing the background counts. Consequently, an imaging detector that has higher spatial resolution and lower background counts is desired for Pu particle detection.

The Si-PM-based GGAG imaging detector presented in this paper resembles one developed for alpha particles (Morishita et al., 2014, 2017), but we use a ceramic scintillator (GGAG) for the detector. Much better performance is expected for the Si-PM-based GGAG imaging detector than that with an Si-PM array combined with a single-crystal GAGG plate (Morishita et al., 2014, 2017), since higher spatial resolution was obtained for the PSPMT-based GGAG imaging detector than that of a GAGG-based detector (Yamamoto and Nitta, 2018).

Another new feature of the proposed Si-PM-based GGAG imaging detector is its capability to achieve simultaneous imaging and

* Corresponding author.
E-mail address: s-yama@met.nagoya-u.ac.jp (S. Yamamoto).

https://doi.org/10.1016/j.radmeas.2018.09.011
Received 4 July 2018; Received in revised form 18 September 2018; Accepted 19 September 2018
Available online 20 September 2018
1350-4487/

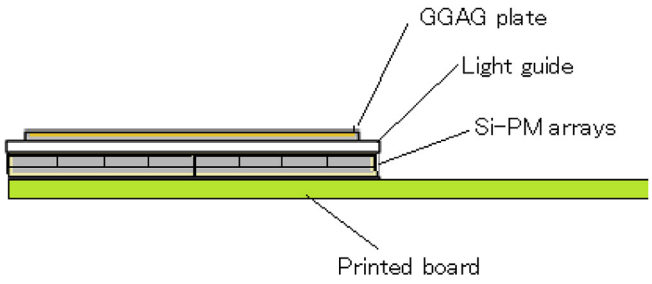

Fig. 1. Schematic drawing of proposed Si-PM-based GGAG imaging detector.

separation of different types of radiation. Some scintillators, such as a plastic scintillator or GAGG, showed different decay times for different types of radiation (Winyard et al., 1971; Kubota et al., 1999; Wolszczak and Dorenbos, 2017; Kobayashi et al., 2012; Tamagawa et al., 1971). We found that GGAG also has different decay times for different types of radiation and that the images could be separated by pulse-shape discrimination. We measured GGAG's decay times for alpha particles, beta particles, and gamma photons and separated the images of different types of radiation using pulse-shape discrimination. The separation of alpha particles from beta particles or gamma photons will contribute to achieving Pu detection with lower background counts.

2. Methods

2.1. Si-PM-based GGAG imaging detector

In the proposed Si-PM-based GGAG imaging detector (Fig. 1), a GGAG plate was used as the scintillator. A light guide is inserted between the scintillator and Si-PM array to distribute the scintillation light among the several channels of the Si-PM array, thus helping to properly calculate the position based on the Anger principle. The Anger principle is applied in a position-calculation method that calculates gravity using several voltage signals of the Si-PM channels near where the radiation is detected. This principle is commonly used in scintillation cameras (so-called Anger cameras) (Yamamoto et al., 2011) and PET detectors (Yamamoto et al., 2010, 2013). The Si-PM array detects the scintillation light produced by the interaction between radiation and the GGAG plate.

A photo of the proposed Si-PM-based GGAG imaging detector without a reflector is shown in Fig. 2. The size of the GGAG plate was 20 mm × 20 mm, with 0.5 mm thickness. It was optically coupled to an 8 x 8-channel Si-PM array made of 4 sets of commercial Si-PM arrays (3 mm × 3 mm channel size arranged 4 x 4, Hamamatsu Photonics, MPPC S12642-050) arranged 2 x 2. A 1-mm-thick light guide was used between the GGAG plate and the Si-PM arrays to distribute the scintillation light among the channels of the Si-PM arrays. The thickness of the light guide was set based on our data obtained for the PSPMT-based GGAG imaging detector (Yamamoto and Nitta, 2018). Silicone rubber (Shin-etsu Silicone, KE-420) was used for the optical coupling. For the reflector, aluminized Mylar was used because we measure the performance of the imaging detector mainly for alpha particles.

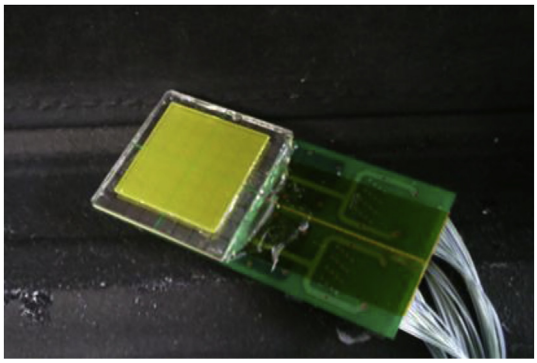

Fig. 2. Photo of proposed Si-PM-based GGAG imaging detector: without aluminum Mylar.

The signals from the 64 channels of the 8 x 8 Si-PM array were fed to the amplifiers of the data acquisition electronics using fine coaxial cables for calculating the position and energy as well as pulse-shape discrimination. To minimize the effect of the Si-PM's high capacity, the current signals from each Si-PM channel were transferred to a weighted summing board, terminated by 25 Ω registers, and converted to voltage signals. The voltage signals were individually amplified by voltage-feedback high-speed (bandwidth: 300 MHz; slew rate: 1400 V μs^{-1}) operational amplifiers (AD 8056, Analog Devices) and summed for rows and columns using summing amplifiers. We maintained a constant room temperature during measurements. Breakdown voltage of the Si-PM was ~-53 V, and we supplied ~-54 V during alpha particle measurements. For the measurements of lower-energy gamma photons and X-ray, we increased the supplied voltages to obtain the proper pulse heights.

The weighed sum signals were fed to 100-MHz analog-to-digital (A-D) converters in the data acquisition system and integrated digitally with two different integration times (full integration and partial integration) to calculate the energy spectra and pulse-shape spectra. For the energy spectra, the full integration value was used, while for the pulse-shape spectra, the ratio of partial to full integration values was used (Yamamoto et al., 2010; Yamamoto, 2008).

2.2. Spatial resolution measurements

Spatial resolution for alpha particles was evaluated using a tungsten slit mask having slits with 1.6 line pair (lp)/mm (0.31 mm slit width) to 3.2 lp/mm (0.156 mm slit width) as shown in Fig. 3 (A). The mask was made of 0.2-mm-thick tungsten and used to evaluate the spatial resolution for alpha particles. Spatial resolution for gamma photons, X-ray, and beta particles was evaluated using a slit mask of 2-mm-thick tungsten, which has 0.3-mm to 0.6-mm slit widths (Fig. 3 (B)).

We evaluated the spatial resolution for the Am-241 alpha source (5.5 MeV) (15-mm diameter), Sr-Y-90 beta particles (maximum energy: 2.28 MeV, distributed over ~3-cm-diameter area with many spots), Ca-45 beta particles (maximum energy: 0.24 MeV, ~5 mm in diameter), Co-57 gamma photons (122 keV, point source), Am-241 gamma phones (60 keV, 15 mm in diameter), and Cs-137 low-energy X-ray (~35 keV, point source). To evaluate the spatial resolution for alpha particles, we set the tungsten slit mask shown in Fig. 3 (A) on the imaging detector's surface and irradiated alpha particles in close proximity to the tungsten slit mask. For our evaluation of the spatial resolution of beta particles, gamma photons and X-ray, we set the slit mask shown in Fig. 3 (B) on the imaging detector's surface and carried out the respective irradiation ~2 cm from the detector's surface.

2.3. Energy-resolution measurements

Energy resolution was evaluated by setting a region of interest (ROI) on the images measured for the evaluation of spatial resolution, and the energy distribution was derived. The ROIs were set at the central parts of the images. From the derived energy distribution, energy resolution was estimated for alpha particles, gamma photons, and X-ray.

2.4. Decay-time measurements

The pulse shape was measured with a digital oscilloscope (Yokogawa DLM2052: maximum sampling rate 500 MHz, 2.5 GS/s). The output of the weight-summing circuit was fed to the digital oscilloscope, and average pulse shapes were measured for alpha particles (Am-241), gamma photons (Cs-137), and beta particles (Sr-Y-90). We individually plotted the data on a graph and evaluated the decay times.